Observations of the plume generated by the December 2005 oil depot explosions and prolonged fire at Buncefield (Hertfordshire, UK) and associated atmospheric changes

T. A. MATHER[1], R. G. HARRISON[2], V. I. TSANEV[3], D. M. PYLE[1], M. L. KARUMUDI[2], A. J. BENNETT[2], G. M. SAWYER[3] AND E. J. HIGHWOOD[2]

[1] *Department of Earth Sciences, University of Oxford, Parks Road, Oxford OX1 3PR, UK.*

[2] *Department of Meteorology, University of Reading, P.O. Box 243, Earley Gate, Reading RG6 6BB, UK.*

[3] *Department of Geography, University of Cambridge, Downing Place, Cambridge CB2 3EN, UK.*

Summary

The explosions and subsequent fire at the Buncefield oil depot in December 2005 afforded a rare opportunity to study the atmospheric consequences of a major oil fire at close range, using ground-based remote sensing instruments. Near-source measurements (<10 km) suggest that plume particles were ~50% black carbon (BC) with refractive index 1.73-0.42i, effective radius (R_{eff}) 0.45-0.85 μm and mass loading ~2000 μg m^{-3}. About 50 km downwind, particles were ~60-75% BC with refractive index between 1.80-0.52i and 1.89-0.69i, R_{eff} ~1.0 μm and mass loadings 320-780 μg m^{-3}. Number distributions were almost all monomodal with peak at r<0.1 μm. Near-source UV spectroscopy revealed elevated trace gas concentrations of SO_2 (70 ppbv), NO_2 (140 ppbv), HONO (20 ppbv), HCHO (160 ppbv) and CS_2 (40 ppbv). Our measurements are consistent with others of the Buncefield plume, and with studies of the 1991 Kuwaiti oil-fire plumes; differences from the latter reflecting in part contrasts in combustion efficiency and source composition (refined fuels vs. crude oils) leading to important potential differences in atmospheric impacts. Other measurements made as the plume passed overhead ~50 km downwind showed a reduced solar flux reaching the surface but little effect on the atmospheric potential gradient (electric field). The wind speed data from the day of the explosion hints at a possible explosion signature.

Keywords: oil fire plume; atmospheric particles; black carbon; trace gases; solar radiation; potential gradient

1. Introduction

Following a large explosion at the Buncefield oil depot, (southern UK, figure 1), on December 11th 2005 a major oil-fire burned for 3 days. This was probably the largest fire in the UK since 1945, and offered a rare opportunity for ground-based measurements of the composition and consequences of a major smoke plume at close range, with the aim of better understanding the potential atmospheric and environmental perturbations of such events.

The main previous studies of emissions from large oil fires followed the 1991 Gulf war when Kuwaiti oil wells were ignited (see Hobbs & Radke 1992 and special issues of *J. Geophys. Res.*, **97**(D13), 1992 and *Atmos. Environ.*, **28**(13), 1994). At the time there was concern that these plumes would have a global impact, with nuclear-winter type scenarios, diversion of monsoons and harvest failure suggested (Brimblecombe 1994). However aircraft measurements of the plume suggested limited potential for such far-reaching effects as (i) the particle emissions were less than expected, (ii) the smoke was not as black as expected (more efficient combustion), (iii) the smoke was not carried high into the atmosphere, and (iv) the smoke had a short atmospheric residence time (Hobbs & Radke, 1992). Regional effects, however, included impacts on cloud properties and formation (Rudich *et al*. 2003), radiative budgets (Pilewskie & Valero 1992), air quality (Amin & Husain 1994) and tropospheric ozone levels (Luke *et al*. 1992).

The chronology and details of the 2005 incident have been summarised in four progress reports of the Buncefield Major Investigation team (Powell 2006a, b, c; Targa *et al*. 2006). The incident was initiated in a major explosion on December 11th at 06:01.32 UT, triggered by the ignition of ~300 tonnes of unleaded petrol, which had overspilled from a storage tank. At the time of ignition, petrol and petrol vapour covered 80,000 m^2, and by the end of the incident, 21 storage tanks had been damaged or destroyed.

The initial explosion caused wide damage to buildings, with a shock wave pressure of 700–1000 mbar close to source; and 7–10 mbar at 2 km distance. Impulsive waves from the explosion were recorded by British Geological Survey seismometers up to 300 km away. The air pressure wave was recorded on seismometers up to 200 km distance. Eyewitness reports mention the possibility of other explosions, but none left a seismic record (Powell 2006c). The explosion was assigned a seismic magnitude (M_L) of 2.4, corresponding to a seismic energy release of about 1.8×10^9 J.

The explosion was followed by a major fire, which burnt strongly for the first 30–36 hours (according to fire officers, the peak was at about noon on December 12th), and was eventually extinguished late on 14th December (Anon 2006). For the first two days of the incident (11th and 12th December), the fire produced a sufficiently strong thermal image to be detected by automated fire detection algorithms on the Moderate Resolution Imaging Spectroradiometer (MODIS) satellites (web fire mapper, http://maps.geog.umd.edu/default.asp).

At the time of the explosion, fuel storage tanks on the Buncefield site held 8.2×10^7 kg of unleaded petrol, aviation fuel and diesel; about 2/3 of the inventory (5.6×10^7 kg) was burned during the incident (Targa *et al*. 2006). The Kuwaiti oil fires burned at rates estimated from 0.17 to 0.55 Mt day^{-1} (Johnson *et al*. 1991). Therefore, the Buncefield conflagration burned at about 3-10% of this rate. During control and containment operations of the Buncefield fire, 2.5×10^5 l of foam concentrate (including, among others, zinc and perfluorooctane sulphonate, PFOS) and 2.5×10^7 l of water were used (Powell 2006a,b).

The incineration of 5.6×10^7 kg of fuel would have released 2.5×10^{15} J of thermal energy at a rate of ~10^{10} W for 3-4 days. The expected rise height for the buoyant plume of combustion products in a standard atmosphere is 2-3 km (Morton *et al*. 1956; p 20), while the initial conflagration of ca. 3×10^5 kg of spilled fuel (with a potential thermal energy release of 10^{13} J) would have formed a plume up to 3.5 km high (Morton *et al*. 1956; p 21), consistent with NAME modelling and satellite imagery (Targa *et al*. 2006).

At the time of the explosion, local temperatures were around freezing, wind-speeds were low and anti-cyclonic conditions prevailed (Jones *et al*. 2006). There was a strong inversion layer in the atmosphere, which trapped the lofted plume and its products at a moderate altitude. The first day following the explosion was marked by the formation of a dark plume which spread slowly across a wide area of southern England, as viewed from the ground and weather satellites. On 12th December, wind-speeds increased and, coupled with the diminishing strength of the fires, the plume became more narrowly defined. Despite the unprecedented scale of the Buncefield explosion and fire, ground-level concentrations of a range of pollutants remained low to moderate over local, regional and national scales. It appears that the high plume buoyancy and favourable meteorological conditions meant that the plume was trapped aloft, with minimal mixing to the ground (Targa *et al*. 2006).

While the Buncefield event was a disaster for the local residents with over 40 injured and more than 2000 evacuated, it offered a rare opportunity for atmospheric scientists to observe the effects of an event of this type and scale. In this instance, a fortuitous combination of timing and meteorological conditions limited the potential impacts on the regional terrestrial environment and human health, but observations of the atmospheric consequences of such an event are of interest for comparison with past and predicting the consequences of future events. Here we present a portfolio of opportunistic ground-based measurements made in the days following the fire, both close to the oil depot and more distal from it. As well as further assessing the atmospheric consequences of the plume, these observations demonstrate the potential of ground-based techniques to complement the airborne measurements (see Targa *et al*. 2006 for more details of the airborne measurements of the Buncefield plume) when responding to such crises.

2. Measurements and methods

2.1 *Near-source measurements*

Measurements were made close to the oil depot on 12th and 13th December from sites shown in the inset to figure 1.

2.1.1 *Sun photometer measurements*

Sun photometer measurements were made on 13th December at two sites viewing through the plume (A1 and A2) and two sites viewing through the background atmosphere (BGA1 and BGA2, figure 1), in order to characterise the number density, size distribution and composition of particles in the smoke plume. Measurements were made with a hand-held Microtops II sun photometer which measured direct solar radiance in five channels with peak wavelengths of 380, 440, 675, 936 and 1020 nm. The amount of Precipitated Water Vapour (PWV) was evaluated using the 936 nm channel of MICROTOPS II and the standard procedure provided by the manufacturer, Solar Light Co.

Ångström coefficients and size distributions were calculated by regression analysis and using King's algorithm (King *et al*. 1978; King 1982) for the inversion of aerosol spectral attenuation data respectively, as described in more detail elsewhere (Mather *et al*. 2004). The inversion starts with an initial estimate of the Junge distribution parameter ν based on the Ångström exponent α. This is iteratively modified until the final solution satisfies both the coincidence of measured ($\tau_a = \tau_{total} - \tau_{background}$) and calculated aerosol optical thicknesses (τ_a) within the experimental noise level and the positivity constraint. The success of the inversion is characterised by three interrelated quantities: the covariance matrix of relative errors E_{rel}; the sample variance of the regression fit (ε^2); and the number of coincidences M_c between retrieved and measured aerosol optical depth within error. A more sophisticated and powerful algorithm, based on measurement of direct and scattered solar radiation (Dubovik & King 2000), could not be applied due to the strong inhomogeneity of fire plumes.

There are some practical difficulties when applying King's method to our data. *A priori* knowledge of the Mie extinction efficiency factor $Q(r, \lambda, m)$ within the considered radius interval (r_{min}, r_{max}) is required, i.e., the aerosol must be assumed to be of homogeneous spherical particles with a known single index of refraction. External mixtures are thus excluded from consideration (c.f. Lesins *et al*. 2002).

Airborne measurements of particles in the plumes from the Kuwaiti fires showed that different plumes contained particles of different compositions. White smoke plumes contained ~4% soot; black plumes ~20-25% soot, while plumes associated with

burning oil fountains in the desert had up to 48% soot. After mixing, the composite plume particles comprised ~30% salt (with surprising large amounts of NaCl), 15-20% soot, 8% sulphate and ~30% organics. Larger particles included oil droplets (which tended to rain out close to the source) and chain aggregates (Hobbs & Radke 1992). The majority of the particles formed cloud condensation nuclei (CCN). The smoke in the Buncefield plume was produced by burning of oil fuel, which was partially extinguished with water and aqueous film-forming foams (AFFF). Airborne measurements of the plume showed that the main constituent of the plume was black carbon (Targa *et al*. 2006); however aerosol particles are also likely to include unburned or partially oxidised fuel (organic carbon), water droplets and AFFF and its by-products. The colour of the smokes was mainly black or brownish, but some bright parts were also observable depending on plume's geometrical depth or as a result of drift caused by wind shear (electronic appendix, figure A). Given the lack of precise compositional information for particles in the Buncefield plume, inversions were tested for different indices of refraction over the maximum range of radii (0.08-4 μm).

Calculations of the optical properties of an internal mixture of components requires the use of a mixing rule to compute the appropriate effective composite refractive index (Chylek *et al*. 2000). The best mixing rule will depend on the geometric arrangement of the components comprising the mixture (Lesins *et al*. 2002). We modelled the Buncefield smoke as water droplets (*W*) enclosing black carbon (*BC*) particles (inclusions) and used the Maxwell-Garnett mixing rule (Bohren & Huffman 1983) to calculate the effective dielectric constant ε_m:

$$\varepsilon_m = \varepsilon_W \frac{\varepsilon_{BC} + 2\,\varepsilon_W + 2\,f_{BC}\,(\varepsilon_{BC} - \varepsilon_W)}{\varepsilon_{BC} + 2\,\varepsilon_W - f_{BC}\,(\varepsilon_{BC} - \varepsilon_M)} \qquad (1),$$

where $\varepsilon_W = 1.8 - 0.0i$ and $\varepsilon_{BC} = 3.0 - 4.0i$ are the complex dielectric constants (the square of the refractive index) and f_{BC} is the volume fraction of inclusions (Horvath 1993). The values of $Q(r, \lambda, m)$ can then be evaluated using King's approach. Schuster *et al*. (2005) used three mixing models (concentric spheres, Maxwell Garnett, and external mixture) to calculate mass absorption efficiencies of some AERONET non-dust size distributions (Dubovik *et al*. 2002) and showed that for f_{BC}

>0.5 all three mixture models were essentially similar, and converged to the same mass absorption efficiency value of 2.8 m^2 g^{-1} as f_{BC} approached one.

In the absence of any prior data for the volume fraction f_{BC} of the Buncefield smoke plume, tests were run to establish the index of refraction that gave the best agreement between the measurements and the inversion using the three measures $E_{rel}(f_{BC})$, $\varepsilon^2(f_{BC})$ and $M_c(f_{BC})$.

2.1.2 *UV measurements of plume composition*

Gas spectroscopic measurements were made with two small UV spectrometers (Ocean Optics S2000, range 238-385 nm, and USB2000, range 253-404 nm), each coupled by a quartz fibre optic bundle to a 25 mm diameter quartz-lens telescope (field of view 8 mrad). A specially designed JScript working in the DOASIS environment (http://www.iup.uni-heidelberg.de/bugtracker/projects/doasis/) was used to record automatically spectra from the USB2000 with maximum amplitude, without any saturation and with total integration time (spectrum integration time × number of co-adds) of 5 s. The amplitudes of spectra depend mainly on the time variation of the down-welling zenith scattered solar radiation. Spectra from S2000 were collected using the time acquisition mode of Ocean Optics OOIBase32 software and manually adjusting the integration time and number of co-adds.

Measurements were made from four locations on 12th and 13th December 2005 (figure 1). In all cases the viewing geometry was close to vertical with zenith angles less than 40°. On both days, temperature and humidity profiles were similar. Position UV1 (12th December, 13.29-14.31 UT) was 5.95 km distant from the fire, and the estimated plume age was 6.3-8.3 min based on mean wind velocity data from Larkhill air sounding station (Station 03743, http://weather.uwyo.edu/upperair/sounding.html). The plume at this time had two parts: one part was dark, non-transparent and of variable density, with strong variations in the intensity of registered spectra. The second part was also dense, but more uniform and grey in colour. Spectra from these two parts of the plume are denoted HH1 and HH2. At position BGUV1 (13th December), we measured background (i.e., atmospheric columns not influenced by the fire emissions) gas column amounts under a cloudy sky. At point UV2 (13th

December, 10.53-12.01 UT; 5.40 km distant from the fire; plume age 5.3-7.0 min) the plume was dense and non-transparent but relatively homogeneous (dataset HH3), whilst at point UV3 (13th December, 12.37-13.10 UT, 5.72 km distant from the fire; plume age 6.0-7.9 min), the plume was transparent, brown and less homogeneous (dataset HH4). At this location we measured background gas column amounts by pointing the telescopes towards clear sky. At point UV4 (13th December, 13.31-14.14 UT; 0.78 km distant from the fire; plume age 0.8-1.1 min), the plume was transparent but strongly bifurcating (dataset HH5).

Gas column amounts were evaluated using the DOAS method (Platt, 1994) implemented in WinDOAS software (Van Roozendael & Fayt 2001). A background spectrum from the set closest in time to each measurement set was used in this evaluation. As this time interval was at most ~1-2 hours, it is assumed that, other than the influence of the fire, the rest of the atmospheric column (including the stratosphere) is approximately constant. The most precise cross sections from the HITRAN database (Orphal & Chance 2003) for the following gases were included in the fit: SO_2 (Rufus *et al*. 2003), NO_2 (Vandaele *et al*. 1998), nitrous acid (HONO, Stutz *et al*. 2000), formaldehyde (HCHO, Cantrell *et al*. 1990) and CS_2 (Schneider & Moortgat, http://www.science-softcon.de/uv-vis.htm). First and second order Ring effect cross sections were included as additional pseudo-absorbers (Chance & Spurr 1997). The selected fitting windows were 309-330 nm (all gases) and 330-380 nm (all gases excluding SO_2). The amount of straylight is higher within the first window but it is favourable for retrieving SO_2 column amounts. The results for other gases coincide within retrieval confidence intervals (mean ± three standard deviations), but errors in short wavelength windows are usually much higher. For this reason, we use SO_2 column amounts derived from the short wavelength window, and column amounts of other gases from the long wavelength window.

An example retrieval result is shown in figure 2. The residual usually contained a weak and unidentified structure (black line on panel B in figure 2). This structure does not correspond to the well-known absorbers within used fitting windows. It should be noted that the absorption spectra of all aromatic hydrocarbons have prominent bands below 300 nm (Platt 2000). Similar methods have been used to measure SO_2, NO_2,

HCHO, HONO and CS_2 previously in biomass, coal furnace and gas-fired power station plumes as well as the ambient atmosphere (Stutz *et al*. 2000; Oppenheimer *et al*. 2004; Yu *et al*. 2004; Heckel *et al*. 2005; McGonigle *et al*. 2005). These trace gas species, as well as being pollutants, are important in the chemistry of combustion plumes (Trentmann *et al*. 2003; Yu *et al*. 2004).

2.2 *Plume arrival measurements at University of Reading meteorology department*

The oil fire plume arrived over the University of Reading (figure 1), ~50 km away from the oil depot, at about 11:15 UT on Sunday 11th December, as shown by the darkening of the sky (electronic appendix, figure A). During the day, the appearance of the plume varied, but at sunset there was an oily appearance to the sky.

2.2.1. *Sun photometer measurements*

Sun photometer measurements were made from the roof of the University of Reading Meteorological Department, as the plume came over on Sunday 11th December 2005. In this case the Microtops II sun photometer used measured direct solar radiance in five channels with peak wavelengths of 380, 440, 675, 936 and 1020 nm. Data were processed as described above (section 2.1.1).

2.2.2 *Solar radiance measurements*

Measurements of solar radiation are routinely made at Reading University Atmospheric Observatory (http://www.met.rdg.ac.uk/~fsdata/obshome.html) using Kipp and Zonen CM5 thermopile pyranometers, which generate a voltage. The pyranometer voltages are each amplified (Harrison & Knight 2006) and recorded automatically as 5-minute averages. The total (or "global") irradiance G and "diffuse" (scattered) irradiance D are both recorded, with D obtained using a shade ring to block the direct solar beam. A shade ring correction is applied to compensate for the diffuse radiation obstructed by the shade ring, which varies with time of year (Steven & Unsworth 1980).

More insight can be gained by normalising the D and G data. For a measurement of the diffuse radiation D and simultaneous measurement of global radiation G, the instantaneous *diffuse fraction* (DF) is given by

$$DF = \frac{D}{G} \quad (2).$$

This typically varies between DF ~ 0.2 in cloud free conditions to DF = 1.0 in completely overcast conditions (Harrison & Stephenson 2006). A further normalised quantity that can be determined is the clearness index K_t (Muneer 1997), defined as

$$K_t = \frac{G}{E} \quad (3),$$

where E is the solar radiation at the top of the atmosphere. E is given by

$$E = S_0 \cos Z \quad (4),$$

for S_0 the solar constant (1366 W m^{-2}) and Z the solar zenith angle for the day of the year and the position of the observation (Yallop 1992).

2.2.3 *Potential gradient (PG) measurements*

A vertical conduction current flows in the atmosphere as a result of the global atmospheric electric circuit, maintained by global thunderstorm and shower cloud activity (Chalmers 1967). This is linked to a surface electric field, conventionally measured as the potential gradient, PG. It is well established that clouds and aerosol modify the local atmospheric electrical parameters, and that combustion itself often generates smokes that are electrically charged (Green & Lane 1957). Because of the possible effects of charge on aerosol formation, coagulation and in-cloud aerosol removal (Harrison & Carslaw 2003), it is useful to monitor electrical changes associated with large fire plumes like that from Buncefield.

At the Reading University Atmospheric Observatory, the PG is measured routinely using an electrostatic field mill (Chubb Instruments, model JCI131) viewing upwards from 2 m above the surface. The response time of the instrument is rapid (~4 milliseconds), with measurements logged every second. Electric field measurements obtained are calibrated to the undistorted PG at a reference height of 1 m (Bennett & Harrison 2006).

2.1.4 Surface *wind measurements*

Wind speed and surface atmospheric pressure are measured continuously at Reading Observatory (http://www.met.rdg.ac.uk/~fsdata/obshome.html). The wind speed sensors are two voltage output Vector Instruments A100 cup anemometers, one

mounted on an instrument tower at 10 m and the other mounted on an adjacent 2 m mast. Pressure is measured using an analogue output Druck DPI150 precision barometer, which operates on the oscillating drum principle. The A100 cup anemometer is sensitive, with a specified starting speed of 0.2 m s^{-1} and stopping speed 0.1 m s^{-1}. It has a response length of 5 m ± 10%, and the voltage output module has an exponential time constant of 0.15 s. Both the cup anemometer and barometer are sampled at 1 Hz, using 12 bit analogue to digital resolution. This method for routine recording degrades the 0.01 hPa measuring resolution of the precision barometer to 0.1 hPa, but it is necessary to permit the full range of atmospheric pressures commonly encountered to be measured.

3. Results and discussion

3.1 *Sun photometer measurements*

Anthropogenic aerosol emissions play a role in global climate change through both the direct and indirect effect (e.g., Charlson *et al*. 1992). Particles can also play a key role in the chemical reactions occurring in fire plumes both by providing surfaces for heterogeneous chemistry (e.g., in the Kuwaiti oil plumes the presence of particles resulted in rapid depletion of SO_2 and NO_x; Ferek *et al*. 1992) and by affecting a plume's thermal and radiative properties (Trentmann *et al*. 2003). To understand the potential impact of events such as the Buncefield as a contribution to regional and global scale radiative budgets parameters such as the optical properties, size distribution and composition of the aerosol emissions are important. Targa *et al*. (2006) used emission factors and estimates of the mass of fuel consumed to estimate that the Buncefield event emitted ca. 8250 Mg of PM_{10}, or ~6% of annual UK emissions in 2003. Here we present our sun photometer measurements and discuss what they suggest about the optical properties, size distribution, composition and evolution downwind of the Buncefield aerosol.

3.1.1 *Near-source plume measurements*

Figure 3a shows the total optical thicknesses recorded by the sun photometer at the near source sites. There is a clear increase in the total optical thicknesses through the plume as opposed to the background atmosphere. Data were grouped into sets of 3 to 5 adjacent measurements in order to quantify the variation in the signal due to the

plume's variable structure (as shown for site A2 in figure 3b). Measurements from BGA1 were taken as $\tau_{background}$ for A2. The Ångström parameter, α, ranges from 0.30 to 0.48 for A2 (figure 3b). Mean α was 0.42 and the mean dispersions within the groups of data were 0.05, 0.04, 0.04, 0.03 for the aerosol optical thicknesses (τ_a) at λ = 440, 675, 870 and 1020 nm respectively. For the earlier measurement site (A1) the last 14 measurements were taken to represent the background atmosphere as the plume swung away from the sun during the period of the measurement. Visual observations at the time suggested that there was some cirrus cloud between the plume and the sun, but this background was homogeneous after 11:28 UT. Mean α was 0.14 and the mean dispersions within the groups of data for τ_a were 0.03, 0.03, 0.02, 0.02 respectively, at λ = 440, 675, 870 and 1020 nm.

Using the α values, the mean through-plume optical thickness values ($\tau_a(\lambda)$) and the calculated dispersions, retrievals were carried out using indices of refraction calculated according to (1) for $0 \leq f_{BC} \leq 1$. Figure 4 shows that functions $E_{rel}(f_{BC})$ and $\varepsilon^2(f_{BC})$ have minima at f_{BC}~0.5. At f_{BC}~0.5, $M_c(f_{BC})$~4 suggesting (see section 2.1.1) complete coincidence between the model and the measurements to within error. This suggests that for the near-source measurements the particles were ~50% BC and 50% water by volume. As discussed above, for $f_{BC} \geq 0.5$ all internal mixture models are equivalent, which lends further confidence to our results. Further, the results presented in Table 1 show that in the range $0.5 \leq f_{BC} \leq 0.75$ there is good agreement for the retrieved values of both columnar number density of particles (CND) and R_{eff}. Taking the median values it is reasonable to conclude that CND of 1.1×10^8 and 5.3×10^8 particles cm^{-2} and R_{eff} of 0.85 and 0.45 μm are appropriate for A1 and A2 respectively. The geometry of the sun and the plume during 13th December (the plume swung from the south-west to south-east sector during the day) was such that the estimated plume age was approximately the same at both A1 and A2 (estimated at 5-8 min). Differences between the two sets of measurements are therefore more likely to reflect differences in fire fighting activities and background meteorology at the time of measurement, rather than evolution of the aerosol plume during transport. Given the PM_{10} emission estimates and a black carbon volume fraction of ~50%, this suggests that the BC emissions from the event might have been ~5500 Mg.

The particle size distributions and spectral dependency of single scattering albedo $\omega(\lambda)$ for f_{BC} = 0.5 are shown in figure 5. In figure 5a it can be seen that data groups N and O had fewer large particles. These data groups represented observations of the plume edge as the plume swung away from the sun. However, it should be noted that the exact shape of retrieved aerosol number, surface and volume distributions was sensitive to the choice of index of refraction.

Figure 6 presents time variations of aerosol columnar number density (CND) and precipitated water vapour (PWV) within plume observed at A2. The values of PWV (about 12 mm) are almost half the PWV estimated for whole atmospheric column (upper air sounding data from Larkhill), i.e., the smoke was very rich in water vapour substantiating our model of an internal mixture of water droplets with BC inclusions.

3.1.2 *Distal plume measurements*

Figure 7a shows the total optical thickness on 11th December 2005 over Reading. There is a clear increase in the aerosol optical depth in all the wavelengths after 12:40 UT, reflecting the plume arrival in between the sun photometer operator and the Sun.

Mean α was 0.09 over Reading. Table 2 shows that the best agreement between the data and the retrieved results is obtained for f_{BC} =0.60-0.75, giving a mean particle loading of (0.70-0.84)×10^{8} particles cm^{-2} and R_{eff} of ~1.0 μm. The particle size distributions for f_{BC}= 0.65 are shown in figure 7b. As discussed above, for $f_{BC} \geq 0.5$ all internal mixture models are equivalent.

3.1.3 *Comparison of measurements from the 2 sites and with previous measurements*

The Ångström coefficients, α, measured for the Buncefield plume are characteristic of a coarse aerosol (Baltensperger *et al*. 2003). Values of α for the distal aerosol (Reading) are lower than for the near-source aerosol, reflecting the slightly larger size of the aerosol at Reading, and consistent with the R_{eff} values at the different locations (Tables 1 and 2). The column number density of the distal aerosol is slightly less than at the proximal sites, however the increase in the aerosol size means that the columnar volume loading of the aerosol is similar at both distances from the source. Since measurements were made on different days, we cannot be sure that the fire or the

meteorological conditions were exactly comparable, but these observations coupled with the increase in BC volume fraction at the distal site (i.e., suggesting that the aerosol has not taken up water from the atmosphere during transport) suggest particle growth by coagulation during transport on 11th December and that the particles have not been activated as CCN during transport. These measurements are merely suggestive at this stage. Detailed microphysical modelling of the plume during transport on the different days would be needed to understand these plume evolution processes further.

The Automatic Urban and Rural Network (AURN) did not report any elevated levels of PM_{10} at ground level due to the Buncefield fire over the south of the UK. Targeted monitoring (with a Grimm particle sampler) near the oil depot measured a maximum ground level PM_{10} concentration of 985 μg m^{-3} ~2 km from the source. The aircraft measured a $PM_{2.5}$ concentration of 461 μg m^{-3} directly over the source (Targa *et al*. 2006). These measurements are broadly consistent with the retrieved near-source plume particle mass loadings of ~2000 μg m^{-3} (Table 1), especially when we consider that the ground-based measurements may have been of the diffuse plume edge and that the two largest radii in our retrieved size distributions are equivalent to greater than 2.5 μm diameter.

There have been few similar studies of other oil plumes. Pilewskie & Valero (1992) measured optical depths at ~100 km from the Kuwaiti fires, while Nakajima *et al*. (1996) made sun photometer measurement of 1-day old Kuwaiti oil-fire smoke. They recorded τ_a at 500 nm of up to 1.5, and derived a mean α value of ~0.7, mass loading of 590 μg m^{-3}) and a soot fraction of ~16%. Aircraft measurements of Kuwait smoke plumes found particle loadings of ~840 μg m^{-3} (diameter <3.5 μm) 20 km downwind from the source, and >500 μg m^{-3} 150-200 km from source (Hobbs & Radke 1992; Daum *et al*. 1993). The near-source aerosol optical thicknesses and columnar amounts of the Buncefield aerosol (figure 3, Table 1) are consistent with these measurements. The mass loading is slightly higher; reflecting the undiluted nature of this near-source plume. Nakajima *et al*. (1996) suggested that the optical thickness of the Kuwait plume did not change significantly when the plume was spread in weak wind conditions. In the Buncefield plume however, while the optical thickness values of the

distal aerosol (figure 7a) were less than those observed in a 1 day-old Kuwait plume, the estimated plume depth and mass loadings were comparable. At both Buncefield measurement sites, α values are lower than observed for Kuwaiti oil-fire smoke particles. The black carbon content was also higher at both measurement locations than observed in the Kuwait plumes (up to 48%; Hobbs & Radke 1992), plausibly reflecting differences in local meteorological conditions or combustion efficiency. The shape of our size distributions (figures 5 and 7b) agree well with those measured in the Kuwaiti plumes using airborne differential mobility analyser (Hudson & Clarke 1992).

The obtained values of the single scattering albedo $\omega(\lambda)$ (~0.35-0.50, figure 5) are consistent with previous experimental measurements and atmospheric data. Young hydrophobic black carbon soot-water agglomerates had $\omega(\lambda)$-values between 0.35 (at relative humidity, RH=10%) and 0.5-0.6 (at RH=100%) whilst aggregates of hydrophilic soot at any level of RH have albedo about 0.3-0.4 (Mikhailov 2006). The mean single scattering albedo for UK industrial haze varies between 0.4 and 0.6 (Horvath 1993) and for the Kuwaiti oil plumes the single scattering albedo was 0.95 for the white plumes, 0.35 for the blackest plumes and 0.5 to 0.6 for the composite plumes (Hobbs & Radke 1992).

3.2 *Near-source UV measurements*

The column amounts (molecules cm^{-2}) and mixing ratios (ppmv) of NO_2, SO_2, HONO, HCHO and CS_2 measured at different positions are summarised in Table 3. Our near source measurements recorded mean concentrations of SO_2 of ~70 ppbv, NO_2 of ~140 ppbv and HCHO of ~160 ppbv. Near-source aircraft measurements of the Kuwaiti fires found 300-400 ppbv SO_2 and up to 50 ppbv NO_x (Daum *et al*. 1993). By 50 km downwind, SO_2 and NO_x had dropped to 100-500 ppbv and 5-20 ppbv respectively (Hobbs and Radke, 1992). 80 km downwind from Kuwait city, Luke *et al*. (1992) reported HCHO of up to ~22 ppbv. This suggests that the Buncefield plume had comparatively high levels of NO_x and HCHO but lower SO_2 than in the Kuwaiti oil-fire plumes.

Since HCHO is produced by incomplete combustion, its higher levels are consistent with the higher black carbon proportions estimated for the plume particles (see section 3.1) compared to the Kuwaiti plumes. Many of the Kuwait fires were set at naturally pressurised wells (Johnson *et al*. 1991). In contrast, after the initial explosion, the Buncefield plume developed from combustion of a set of fuel-oil ponds. In the former case, there would have been turbulent mixing between crude oil, well gas and oxygen, promoting efficient combustion; in the latter case, combustion efficiency was presumably limited by the rate of advection of oxygen to the pond surface.

The differences in the sulphur and nitrogen species could reflect different sulphur and nitrogen levels in the fuel: the Kuwait crude oils contained ~2.4% S and ~0.14% N (Daum *et al*. 1993), while the Buncefield fuels were refined, with likely S contents from <0.005% (unleaded petrol; Statutory Instrument, 2000) to <0.02% (aviation fuel; Institute of Petroleum, 1998). Our data for the Buncefield plume SO_2/CS_2 molar ratio (0.7-3.9, Table 3) are broadly consistent with measurements of the average SO_2/CS_2 from coal-burning furnaces of 2.1 ± 0.2 (Yu *et al*. 2004).

Estimates of the SO_2 and NO_x depletion rates in the Kuwait plumes ranged from 1-2% hr^{-1} ~100 km from the source (Smyth *et al*. 1994) to 6-22% hr^{-1} in the first few hours after emission (Ferek *et al*. 1992). The rate of depletion of these species has implications in terms of CCN production rate, deposition rates and the range of the impact of the plume (Hobbs and Radke, 1992). Ferek *et al*. (1992) and Herring *et al*. (1996) suggested that reactions on the coarse-mode (desert) soil dust are the key to these high loss rates. While our measurements do not constrain loss rates in the Buncefield plume, we would expect that the lower soil-dust concentrations in the UK plume might have lead to significantly lower loss rates. Combining this with the lower SO_2 emissions, we would expect the Buncefield plume to have had significantly different properties as a source of CCN compared to the Kuwaiti oil plumes.

Targa *et al*. (2006) estimated that the Buncefield event emitted 37.2 Mg of NO_x (or 0.0024% of annual UK emissions in 2003). We can use this value combined with our measured molar gas ratios to NO_2 (Table 4) to make an approximate estimate of the total emissions of other gaseous species from the Buncefield fire. However, a large source of error is introduced as we have not measured the NO/NO_2 ratio in the plume

and in the absence of measurements of plume O_3 this ratio is difficult to estimate. Further, chemical reactions within the plume may cause these ratios to vary. For example, HCHO will be produced via the oxidation of hydrocarbons in the plume, as well as being emitted directly; CS_2 (which can be formed during combustion of sulphur-containing fuels) will be oxidised to SO_2 and COS (Yu *et al*. 2004 and references therein); and HONO is produced by oxidation of NO_x (perhaps involving heterogeneous reactions on the surface of BC particles, see, e.g., Lary *et al*. 1999) and hence is one of the components included in the NO_x emission estimate. Therefore the amount of emitted HONO is not itself estimated. If we assume that the NO/NO_2 ratio lies somewhere between 20 (based on the ~95% NO_x present as NO at the point of emission in power station plumes, Hewitt 2001, with our plume ages were estimated as 1-10 min) and 1 (from measurements in American cities, Logan 1983) and based on mean molar ratios calculated from Table 3 of 0.49 (SO_2), 1.18 (HCHO) and 0.36 (CS_2), the Buncefield event can be estimated to have emitted totals of ~1.2-12.7, 1.4-14.3 and 1.1-11.1 Mg of SO_2, HCHO and CS_2 respectively. For comparison, the reported UK industrial emissions to air in 2005 were 490 Gg (SO_2), 64 Mg (HCHO), 1900 Mg (CS_2) (U.K. Environment Agency Pollution Inventory, http://www.environment-agency.gov.uk/business/444255/446867/255244/). The uncertainty of these values would be reduced should measurements of the NO/NO_2 ratio or the plume O_3 concentrations become available. The low SO_2 emission (1.2-12.7 Mg, compared to ~900 Mg of SO_2 for an equivalent mass of Kuwait oil with an emissions factor of 16 kg kg^{-1}, Laursen *et al*. 1992) is consistent with the considerably lower sulphur contents of the refined fuels burned at Buncefield compared to the heavier oils burned in Kuwait.

3.3 *Solar radiance measurements*

In order to understand the potential for anthropogenic emissions to impact on the Earth's radiation budget, we report solar radiance measurements relating to the effects of the plume. Figure 8a shows measurements obtained using the pyranometer at Reading. In the early part of the day, the diffuse (*D*) and global (*G*) solar irradiances are similar, resulting from a combination of low sun angles, and shade across the measurement site. After 10:00 UT, *D* and *G* diverge with *D* decreasing. The low *D* value from this time until the end of the day illustrates that there is little cloud present,

producing little scattered radiation. Figure 8a shows a small reduction in G around the time that the plume's arrival was observed.

Figure 8b shows the variation in *DF* and K_t during the late morning and early afternoon of 11th December. It is clear that the diffuse fraction *DF* is not changed substantially from clear sky values by the passage of the plume, although there is some reduction between 11:30 and 13:00 UT, consistent with the sun photometer measurements (figure 7a). However, the clearness K_t is reduced steadily from 11:30 UT. This suggests that the particles in the atmosphere were more effective at absorption than scattering, consistent with a black carbon smoke plume. The minimum K_t value is 0.57, reduced from ~0.69 prior to the arrival of the plume. Measurements at Mortimer, Berkshire (~10km from Reading University) suggest that the Buncefield plume decreased the global solar radiation received under it by ~25% (Burt, 2006). For the smoke from the Kuwait oil fires (approximately 100 km downstream of the fires) minimum transmission of solar flux to the surface was 8%, while 78% of the solar radiation was absorbed by the smoke. There was no evidence to suggest significant radiative effects in regions other than those covered by the plume (Pilewskie & Valero 1992).

3.4 *Potential gradient (PG) measurements*

There was no conclusive evidence that the atmospheric PG was influenced by shockwaves from the explosion. Further, no PG anomalies were observed when the plume came over Reading later that day, despite the presence of the large aerosol loadings associated with the plume (section 3.1). This is perhaps surprising given that combustion tends to generate charged particles and the known tendency for aerosol to scavenge ions and increase atmospheric resistance and PG (Harrison & Carslaw 2003).

3.5 *Surface wind measurements*

As mentioned previously, the air pressure wave was recorded on seismometers up to 200 km distant and eyewitness reports mention the possibility of other explosions, but none left a seismic record (Powell 2006c). It would be possible therefore that air pressure waves associated with the explosions might have had an impact on the wind speed measurements at Reading.

The time series of wind speed and pressure measurements obtained at Reading for the hour following the Buncefield explosion was examined. These observations were obtained before sunrise, which occurred after 07:00 UT (see figure 8a). In the 10 m anemometer record, a peak gust of 1.5 m s^{-1} occurred at 06:07 UT, but there was no simultaneous gust measured in the 2 m data. Between 06:00 UT and 07:00 UT, the mean wind speed at 10 m was 0.55 m s^{-1} (standard deviation 0.23 m s^{-1} and skew 0.37). The 06:07 UT gust was the maximum 10 m wind speed value recorded between 06:00 UT and 07:00 UT. An increase in pressure of 0.5 hPa occurred simultaneously with the wind gust, distinguishable above the resolution limit (~0.1 hPa) of the pressure measurements. Seismic records from the British Geological Survey (Powell, 2006c) determine that the main explosion occurred at 06:01:32 UT. The transit time of a sonic wave (330 m s^{-1}) between Buncefield and Reading (~55 km), would be ~166 s, corresponding to an arrival time slightly after 06:04 UT. At Wolverton (~16 km SW of Reading) the seismic wave was detected ~105 s after the explosion and the acoustic wave ~310 s (David Green, pers. comm.). The large change observed at 06:07 UT cannot therefore be unambiguously associated with the explosion, but it is not inconsistent with a subsonic pressure disturbance radiating outwards from Buncefield and passing Reading at 06:07 UT, as acoustic reports of the explosions were made at considerably greater distances.

Further explosions of other tanks occurred after the principal blast at 06:01:32 UT. If the series of wind gusts obtained at Reading 06:07 UT was related to the main explosion, then a similar pattern in wind speed may also have been produced by later explosions. For the 06:07 UT gust, there are in fact two distinct maxima, separated by 49 s. A similar split maximum also occurred around 06:10-06:12 UT.

The pattern in wind speed samples between 06:06 UT and 06:08 UT was compared with the subsequent pattern 06:10-06:12 UT. These two patterns have a correlation of +0.73. A context is needed to understand whether this match readily occurs by chance, or whether it is rare. To provide a quantitative measure of whether the split maximum pattern is common, it was sought in the entire set of 1 Hz wind speed data from the 10 m anemometer, both on the day of the explosion and for the days before and after. A correlation of 0.7 was used as the detection threshold for the pattern of

124 points. On the day before the Buncefield explosion, the pattern did not occur. On the day of the explosion, the pattern occurred 6 times, at 06:10 UT, 08:18 UT, 11:45 UT, 14:40 UT, 19:45 UT and 21:32 UT. On the day after the explosion, the pattern occurred only once, at 17:00 UT.

Coherent patterns repeated in a stochastic variable such as wind speed suggest disturbances having similar histories, either because both sets of fluctuations originated from the same source and propagated over different length paths, or because similar events separated in time caused them both. Either explanation would be consistent with the fluctuations observed at Reading originating from Buncefield explosions, but it is also possible that the local atmospheric conditions on the day concerned were suitable to generate a series of similar coherent structures. This was considered by investigating how commonly the same split maximum pattern occurred within a much longer series of 1 Hz 10 m wind speed data. Measurements at 1 Hz were made using the same A100 instrument, between 7th May 2006 and 13th July 2006. During these 67 days, a wind speed pattern meeting the +0.7 threshold correlation with the Buncefield pattern occurred 151 times, or at a mean rate of 5.7×10^{-5} in any period of 124 points sampled at random. This indicates that, whilst it is clearly possible for the pattern to occur randomly, it is unusual for it to have occurred many times on one day, and highly unusual for it to have occurred twice in a short period, as for 06:06-06:08 UT and 06:10-06:12 UT on 11th December 2005.

4. Conclusions

Our remote sensing measurements of the Buncefield plume have yielded significant insights into its composition. Near-source sun photometer measurements suggest that plume particles were composed of ~50% black carbon (BC) with an index of refraction of 1.73-0.42i, R_{eff} of 0.45-0.85 μm and a plume particle mass loading of ~2000 μg m^{-3}. Although fire and meteorological conditions may have been different on the different measurement days, sun photometer readings ~50 km downwind suggest that particles had grown by coagulation during transport. At this location the particles were estimated to be ~60-75% BC with index of refraction between 1.80-0.52i and 1.89-0.69i, R_{eff} ~1.0 μm and mass loadings of 320-780 μg m^{-3}. The particle number distributions were almost all monomodal with a peak at r<0.1 μm. Our near

source measurements using a UV spectrometer determined mean levels equivalent to 70 ppbv (SO_2), 140 ppbv (NO_2), 20 ppbv (HONO), 160 ppbv (HCHO) and 40 ppbv (CS_2). Based on estimated total NO_x emissions from the event, assumed NO/NO_2 ratios and mean molar ratios with NO_2 of 0.49 (SO_2), 1.18 (HCHO) and 0.36 (CS_2), the Buncefield event can be estimated to have emitted totals of ~1.2-12.7, 1.4-14.3 and 1.1-11.1 Mg of SO_2, HCHO and CS_2 respectively.

Our measurements are broadly consistent with other measurements made of the Buncefield plume and with detailed aircraft studies of the Kuwaiti oil plumes in 1991, although in the latter case there are some interesting differences: (i) our measurements suggest a higher %BC in the Buncefield plume (possibly reflecting differences in local meteorological conditions or combustion efficiency), (ii) we measured a proportionally lower SO_2 content in the Buncefield plume (perhaps consistent with the burning of oil products without contributions from crude oil) and (iii) we measured a proportionally higher HCHO (consistent with less efficient combustion as supported by the higher BC content in the Buncefield plume as well as the probable differences in the combustion style here compared to the Kuwaiti fires) and NO_x content in the Buncefield plume. The Buncefield oil plume was on a much smaller scale than the Kuwaiti fires but these compositional differences might have implications for the comparative atmospheric effects of the plume (e.g., in terms of as a source of CCN).

Other measurements made as the plume passed overhead at Reading (~50 km) from the source showed that the plume reduced the solar flux reaching the surface and that the particles were more effective at absorption than scattering, which is consistent with their origin in an oil fire. The plume had surprisingly little effect on the electrical state of the atmosphere despite the high particle loadings. Analysis of high-resolution wind data from the day of the explosions was also suggestive of a possible signature of an atmospheric disturbance caused by the initial explosions.

Acknowledgements

Dr Fran Fogwill and the NERC Field Spectroscopy Facility are thanked for arranging the rapid deployment of the Microtops II. TAM and VIT gratefully acknowledge the Royal Society for funding and DMP The Leverhulme Trust. The authors thank Claire

Witham (MET office) for useful discussions, Catherine Cosgrove (Energy Institute) and David Green (AWE Blacknest) for information and two anonymous reviewers for their comments on an earlier draft of the paper.

References

Amin, M.B. & Husain, T. 1994 Kuwaiti oil fires - Air quality monitoring. *Atmos. Environ.* **28**, 2261-2276.

Anon 2006 Control of Major Accident Hazards Directive: Major Accident Short Report. Accident GB/2005/001. Published March 8. (http://www.buncefieldinvestigation.gov.uk/reports/rep080306.pdf)

Baltensperger, U., Nyeki, S. & Kalberer, M. 2003 Atmospheric Particulate Matter. In *Handbook of Atmospheric Science* (ed. C. N. Hewitt & A. Jackson), pp. 228-254. Oxford: Blackwell Publishing.

Bennett, A. J. & Harrison, R. G. 2006 *In situ* calibration of atmospheric air conductivity measurements. *Rev. Sci. Instrum.* **77**, 016103.

Bohren, C. F. & Huffman, D. R. 1983 *Absorption and Scattering of Light by Small Particles*. Hoboken, N. J: John Wiley.

Brimblecombe, P. 1994 Introduction: Atmosphere surrounding the Kuwait oil fires. *Atmos. Environ.* **28**, 2137-2138.

Burt, S. 2006 Reduction in atmospheric transparency as a result of the Hemel Hempstead fire, 11-12 December 2005. *Weather* **61**, 156-158.

Cantrell, C. A., Davidson, J. A., McDaniel, A. H., Shetter, R. E. & Calvert, J. G. 1990 Temperature-Dependent Formaldehyde Cross Sections in the Near-Ultraviolet Spectral Region. *J. Phys. Chem.* **94**, 3902-3908.

Chalmers, J. A. 1967 *Atmospheric Electricity*, 2nd edn, Pergamon Press Ltd.

Chance, K. V. & Spurr, R. J. D. 1997 Ring effect studies: Rayleigh scattering, including molecular parameters for rotational Raman scattering, and the Fraunhofer spectrum. *Appl. Opt.* **36**, 5224-5230.

Charlson, R. J., Schwartz, S. E., Hales, J. M., Cess, R. D., Coakley, J. A., Jr., Hansen, J. E. & Hofmann, D. J. 1992 Climate Forcing by Anthropogenic Aerosols. *Science* **255**, 423-430.

Chylek, P., Videen, G., Geldart, W., Dobbie, S. & Tso, W. 2000 Effective medium approximation for heterogeneous particles. In *Light Scattering by*

Nonspherical Particles: Theory, Measurements and Geophysical Applications (ed. M. Mishchenko), pp. 273– 308. San Diego, Calif.: Academic.

Daum, P. H., Al-Sunaid, A., Busness, K. M., Hales, J. M. & Mazurek, M. 1993 Studies of the Kuwait Oil Fire Plume During Midsummer 1991. *J. Geophys. Res.* **98**, 16809-16827.

Dubovik, O. & King, M. D. 2000 A Flexible Inversion Algorithm for Retrieval of Aerosol Optical Properties from Sun and Sky Radiance Measurements. *J. Geophys. Res.* **105**, 20673–20696.

Dubovik, O., Holben, B., Eck, T. F., Smirnov, A., Kaufman, Y. J., King, M. D., Tanre, D. & Slutsker, I. 2002 Variability of Absorption and Optical Properties of Key Aerosol Types Observed in Worldwide Locations. *J. Atm. Science* **59**, 590-608.

Ferek, R. J., Hobbs, P. V., Herring, J. A., Laursen, K. K., Weiss, R. E. & Rasmussen, R. A. 1992 Chemical composition of emissions from the Kuwait oil fires. *J. Geophys. Res.* **97**, 14483-14489.

Green, H. L. & Lane W. R. 1957 *Particulate clouds: dusts, smokes and mists* E&F Spon Ltd, London.

Harrison, R. G. & Carslaw, K. S. 2003 Ion-aerosol-cloud processes in the lower atmosphere. *Rev. Geophys.* **41**, 1012. (DOI 10.1029/2002RG000114.)

Harrison, R. G. & Knight, J. R. 2006 Thermopile radiometer signal conditioning for surface atmospheric radiation measurements. *Rev. Sci. Instrum.* **77**, 116105. (DOI 10.1063/1.2370752.)

Harrison R. G. & Stephenson D. B. 2006 Empirical evidence for a nonlinear effect of galactic cosmic rays on clouds. *Proc Roy Soc A* **462**, 1221-1233. (DOI 10.1098/rspa.2005.1628.)

Heckel, A., Richter, A., Tarsu, T., Wittrock, F., Hak, C., Pundt, I., Junkermann, W. & Burrows, J. P. 2005 MAX-DOAS measurements of formaldehyde in the Po-Valley. *Atmos. Chem. Phys.* **5**, 909–918.

Herring, J. A., Ferek, R. J. & Hobbs, P. V. 1996 Heterogeneous chemistry in the smoke plume from the 1991 Kuwait oil fires, *J. Geophys. Res.* **101**, 14451-14463.

Hewitt, C. N. 2001 The atmospheric chemistry of sulphur and nitrogen in power station plumes. *Atmos. Environ.* **35**, 1155–1170.

Hobbs, P. V. & Radke, L. F. 1992 Airborne Studies of the Smoke from the Kuwait Oil Fires. *Science* **256**, 987-991.

Horvath, H. 1993 Atmospheric light absorption – A review. *Atmos. Environ.* **27**, 293-317.

Hudson, J. G. & Clarke, A. D. 1992 Aerosol and Cloud Condensation Measurements in the Kuwait Plume. *J. Geophys. Res.* **97**, 14533-14536.

Institute of Petroleum 1998 Survey of the average lead and sulphur contents of petroleum products delivered into the UK market, *Petroleum Review*, July, 49.

Israel, H. 1958 The atmospheric electric agitation. In *Recent Advances in Atmospheric Electricity* (ed. L. G. Smith) New York: Pergamon Press.

Johnson, D. W., Kilsby, C. G., McKenna, D. S., Saunders, R. W., Jenkins, G. J., Smith, F. B. & Foot, J. S. 1991 Airborne observations of the physical and chemical characteristics of the Kuwait oil smoke plume. *Nature* **353**, 617-621.

Jones, A., Hort, M., Manning, A., Ryall, D., Taylor, J., Webster, H., Witham, C. & Wortley, S. 2006 The Buncefield oil depot fire: an overview of actual events and the Met Office's dispersion modelling response. *Geophys. Res. Abstracts* **8**, 06452.

King, M. D., Byrne, D. M., Herman, B. M. & Reagan, J. A. 1978 Aerosol Size Distributions Obtained by Inversion of Spectral Optical Depth Measurements. *J. Atmos. Sci*. **35**, 2153-2167.

King, M. D. 1982 Sensitivity of Constrained Linear Inversion to Selection of the Lagrange Multiplier. *J. Atm. Science* **39**, 1356-1369.

Lary, D. J., Shallcross, D. E. & Toumi, R. 1999 Carbonaceous aerosols and their potential role in atmospheric chemistry. *J. Geophys. Res.* **104**, 15929-15940.

Laursen, K. K., Ferek, R. J., Hobbs, P. V. & Rasmussen, R. A. 1992 Emission factors for particles, elemental carbon, and trace gases from the Kuwait oil fires. *J. Geophys. Res.* **97**, 14491-14497.

Lesins, G., Chylek, P., & Lohmann, U. 2002 A study of internal and external mixing scenarios and its effect on aerosol optical properties and direct radiative forcing. *J. Geophys. Res.* **107**, 4094. (DOI 10.1029/2001JD000973.)

Logan, J. A. 1983 Nitrogen oxides in the troposphere: global and regional budgets. *J. Geophys. Res.* **88**, 10785-10807.

Luke, W. T., Kok, G. L., Schillawski, R. D., Zimmerman, P. R., Greenberg, J. P. & Kadavanich, M. 1992 Trace Gas Measurements in the Kuwait Oil Fire Smoke Plume. *J. Geophys. Res.* **97**, 14499-14506.

Mather, T. A., Tsanev, V. I., Pyle, D. M., McGonigle, A. J. S., Oppenheimer, C. & Allen, A. G. 2004 Characterization and evolution of tropospheric plumes from Lascar and Villarrica volcanoes, Chile. *J. Geophys. Res.* **109**, D21303. (DOI 10.1029/2004JD004934.)

Mikhailov, E. F., Vlasenko, S. S., Podgorny, I. A., Ramanathan, V. & Corrigan, C. E. 2006 Optical properties of soot–water drop agglomerates: An experimental study. *J. Geophys. Res.* **111**, D07209. (DOI 10.1029/2005JD006389.)

McGonigle, A. J. S., Thomson, C. L., Tsanev, V. I. & Oppenheimer, C. 2005 A simple technique for measuring power station SO_2 and NO_2 emissions. *Atmos. Environ.* **38**, 21-25.

Morton, B. R., Taylor, G. & Turner, J.S. 1956 Turbulent gravitational convection from maintained and instantaneous sources. *Proc. R. Soc. Lon. A* **234**, 1-23.

Muneer T., 1997 *Solar radiation and daylight models for the energy efficient design of buildings*, Architectural Press.

Nakajima, T., Hayasaki, T., Higurashi, A., Hashida, G., Moharram-Nejad, N., Najafi, Y. & Valavi, H. 1996 Aerosol Optical Properties in the Iranian Region Obtained by Ground-Based Solar Radiation Measurements in the Summer Of 1991. *J. Appl. Meteorol.* **35**, 1265–1278.

Oppenheimer, C., Tsanev, V. I., Allen, A. G., McGonigle, A. J. S., Cardoso, A. A., Wiatr, A., Paterlini, W. & de Mello Dias, C. 2004 NO_2 emissions from agricultural burning in Saõ Paulo, Brazil. *Environ. Sci. Technol.* **38**, 4557–4561.

Orphal, J. & Chance, K. 2003 Ultraviolet and visible absorption cross-sections for HITRAN. *J. Quant. Spectrosc. RA* **82**, 491–504.

Pfeilsticker, K., Erle, F. & Platt, U. 1997 Absorption of Solar Radiation by Atmospheric O_4. *J. Atmos. Sci.* **54**, 933-939.

Pilewskie, P. & Valero, F. P. J. 1992 Radiative effects of the smoke clouds from the Kuwait oil fires. . *J. Geophys. Res.* **97**, 14541-14544.

Platt, U. 1994 Differential optical absorption spectroscopy (DOAS). In *Air Monitoring by Spectroscopic Techniques* (ed. M. W. Sigrist), Chemical Analysis Series, vol. 127, pp. 27–84. New York: Wiley.

Platt, U. 2000 New Approaches of Aromatic Hydrocarbon Measurements by DOAS. In *Proceedings of the Workshop Chemical Behavior of Aromatic Hydrocarbons in the Troposphere*, CEAM, Valencia. (http://www.physchem.uni-wuppertal.de/PC-WWW_Site/pub/valencia2000/proceedings/Platt.pdf.)

Powell, T. 2006a *The Buncefield Investigation. Progress Report.* (http://www.buncefieldinvestigation.gov.uk/report.pdf.)

Powell, T. 2006b *The Buncefield Investigation. Second Progress Report.* (http://www.buncefieldinvestigation.gov.uk/reports/report2.pdf.)

Powell, T. 2006c *The Buncefield Investigation. Third Progress Report.* (http://www.buncefieldinvestigation.gov.uk/reports/report3.pdf.)

Rudich, Y., Sagi, A. & Rosenfeld, D. 2003 Influence of the Kuwait oil fires plume (1991) on the microphysical development of clouds. *J. Geophys. Res.* **108**, 4478. (DOI 10.1029/2003JD003472.)

Rufus, G. S., Smith, P. L., Pickering, J. C. & Thorne, A. P. 2003 High-resolution photoabsorption cross section measurements of SO_2, 2: 220 to 325 nm at 295 K. . *Geophys. Res.* **108**, 5011. (DOI: 10.1029/2002JE001931.)

Schuster, G. L., Dubovik, O., Holben, B. N. & Clothiaux, E. E. 2005 Inferring black carbon content and specific absorption from Aerosol Robotic Network (AERONET) aerosol retrievals. *J. Geophys. Res.* **110**, D10S17. (DOI 10.1029/2004JD004548.)

Smyth, S. B., Peters, L. K., Berkowitz, C. M., Daum, P. H. & Rodgers, M. O. 1994 SO_2 and NO_x conversion rates in the Kuwait oil fire smoke plume. *J. Geophys. Res.* **99**, 16933-16944.

Statutory Instrument 2000 Sulphur content of liquid fuels (England and Wales) Regulations, S.I. no 1460, http://www.opsi.gov.uk/si/si2000/20001460.htm

Steven M. D. & Unsworth, M. H. 1980 Shade-ring correction for pyranometer measurements of diffuse solar radiation from cloudless skies. *Q. J. Roy. Meteor. Soc.* **106**, 865-872.

Stutz, J., Kim, E. S., Platt, U., Bruno, P., Perrino, C. & Febo, A. 2000 UV-visible absorption cross sections of nitrous acid. *J. Geophys. Res.* **105**, 14585-14592. (DOI 10.1029/2000JD900003.)

Targa J., Kent A., Stewart R., Coleman P., Bower J., Webster H., Taylor J., Murray V., Mohan R. & Aus C. 2006 *Initial review of Air Quality aspects of the Buncefield Oil Depot Explosion*, AEA/ENV/R/2168, Issue 1, May 2006.

(www.airquality.co.uk/archive/reports/cat05/0606201126_Buncefield_report_vF3_text2.pdf)

Trentmann, J., Andreae, M. O. & Graf, H. F. 2003 Chemical processes in a young biomass-burning plume. *J. Geophys. Res.* **108**, 4705. (DOI 10.1029/2003JD003732.)

Vandaele, A. C., Hermans, C., Simon, P. C., Carleer, M., Colin, R., Fally, S., Mérienne, M. F., Jenouvrier, A. & Coquart, B. 1998 Measurements of the NO_2 absorption cross-section from 42000 cm^{-1} to 10000 cm^{-1} (238–1000 nm) at 220K and 294 K. *J. Quant. Spectrosc. RA* **59**, 171–184.

Van Roozendael, M. & Fayt, C. 2001 WinDOAS 2.1 Software User Manual, BIRA-IASB, Uccle.

Wagner, T., von Friedeburg, C., Wenig, M., Otten, C. & Platt, U. 2002 UV-visible observations of atmospheric O_4 absorptions using direct moonlight and zenith-scattered sunlight for clear-sky and cloudy sky conditions. *J. Geophys. Res.* **107**, 4424. (DOI 10.1029/2001JD001026.)

Yallop, B. D. 1992 *Technical Note*, Royal Greenwich Observatory, Cambridge.

Yu, Y., Geyer, A., Xie, P., Galle, B., Chen, L. & Platt, U. 2004 Observations of carbon disulfide by differential optical absorption spectroscopy in Shanghai. *Geophys. Res. Lett.* **31**, L11107. (DOI 10.1029/2004GL019543.)

Figure Captions

Figure 1. A map of southern England showing the location of the Buncefield oil depot (in the boxed area; 0.425° W, 51.756° N) and the University of Reading Meteorological Department (cross). Inset shows an enlargement of the boxed area around the oil depot with the measurement sites marked.

Figure 2. An example of fitting process for a spectrum from dataset HH4 with the fit result shown in panel A (the black line is the result of the fit and the grey line is the measured spectrum in units of counts analogue-to-digital-converter). In each other panel the grey line represents the measured differential spectrum minus all fit results related to components other than that mentioned in the panel title and the black line shows the scaled differential cross section (fit result). Panel B: an unidentified structure in the residual observable in almost all registered spectra beneath fire plume. Panel C (optical depth in arbitrary units): the polynomial $P(\lambda)$ (used to remove the low frequency components of absorption spectra) and the offset or ratio $O(\lambda)/L_{bg}(\lambda)$, (where $L_{bg}(\lambda)$ is the background radiance measured under clear sky and $O(\lambda)$ is the third order polynomial compensating for the possible straylight or residual dark current signals). Panel D: the differential optical depth related to the Ring effect and the scaled Ring spectrum. Panels E, F, G and H: CS_2, NO_2, HCHO and HONO fit results and differential cross sections.

Figure 3. (a) Total optical depths measured through the plume near the oil depot on 13th December 2005. The measurements taken after ~11:47 UT at A1 were through the background atmosphere (i.e., without the plume); (b) A detail taken through the plume at site A2, the lines represent how the data was averaged in order to quantify the variability of the plume signal. The mean τ values from BGA1 were deducted from the measured τ values and it is τ_a values that are shown. The calculated α values are marked for each section. Filled diamonds represent τ(440 nm), open squares represent τ(675 nm), open triangles represent τ(870 nm) and crosses represent τ(1020 nm).

Figure 4. The variation for A1 (filled squares) and A2 (open squares) of mean parameters $E_{rel}(f_{BC})$ – dotted lines, $\varepsilon^2(f_{BC})$ – solid lines and $M_c(f_{BC})$ – inset, evaluating the agreement between the measured τ_a values and those from the retrieved size distributions with the Black Carbon (BC) volume fraction f_{BC}.

Figure 5. The retrieved size distributions $dN(\log r)/d\log r$ (lines) and spectral dependency of single scattering albedo $\omega(\lambda)$ (lines with squares) from measurements taken at (a) site A1 for $f = 0.5$ (letters refer to data groupings in time order); (b) site A2 for $f = 0.5$ (letters refer to the data groupings shown in figure 3b).

Figure 6. Comparison of time variation of aerosol columnar number density, CND (line with circles) and precipitated water vapour (line) within plume observed at A2.

Figure 7. (a) Temporal variation of aerosol optical depth over Reading during 11th December 2005. (b) Aerosol size distribution retrieved from the sun photometer measurements at Reading at f_{BC}=0.65.

Figure 8. Solar radiation measurements made at Reading University Atmospheric Observatory on 11th December 2005, together with the screen air temperature (T_d). (a) Global (G) and Diffuse (D) solar irradiance. (b) Short term variations in the diffuse fraction DF (a measure of cloud) and clearness index K_t (a measure of sky clearness). The arrows mark the approximate time of plume arrival.

Short title for page headings

Atmospheric effects of the 2005 Buncefield oil-fire plume

Table 1. Variation of some key retrieved parameters for different values of *f* (the volume fraction of black carbon) for the near plume sites A1 and A2. These are mean values for all the retrievals carried out at these locations.

f	Index of refraction	Mean of retrievals from all groups (figure 1b)		
		Particles cm^{-2} ($\times 10^8$)	R_{eff} (μm)	Total volume of particles[#] ($\times 10^7$ μm^3 cm^{-2})
A1				
0.00	1.33 – 0.00i	0.3	1.2	2.5
0.50	1.73 – 0.42i	1.0	0.9	1.8 (1350)
0.55	1.76 – 0.47i	1.0	0.9	1.8
0.75	1.89 – 0.69i	1.2	0.8	1.5
0.95	1.98 – 0.93i	1.4	0.7	1.4
1.00	2.00 – 1.00i	1.4	0.7	1.3
A2				
0.00	1.33 – 0.00i	1.5	0.9	4.5
0.25	1.53 – 0.19i	4.2	0.5	2.9
0.50	1.73 – 0.42i	5.0	0.5	2.3 (1725)
0.55	1.76 – 0.47i	5.2	0.4	2.1
0.60	1.80 – 0.52i	5.3	0.4	2.0
0.65	1.83 – 0.57i	5.4	0.4	2.0
0.75	1.89 – 0.69i	5.6	0.5	2.4
1.00	2.00 – 1.00i	6.1	0.7	6.6

[#] Values in brackets represent the corresponding approximate mass of aerosol in μg m^{-3} for our best estimate of aerosol composition, assuming an appropriate aerosol density considering a black carbon density of 2 g cm^{-3} (as for the Kuwait oil-fire aerosol, Nakajima *et al*. 1996), water density of 1 g cm^{-3} and a plume depth of 200 m (based on near-source aircraft observations; Targa *et al*. 2006).

Table 2. Variation of some key retrieved mean parameters for different values of *f* (the volume fraction of black carbon) for Reading.

f	Index of refraction	Particles cm^{-2} ($\times 10^8$)	R_{eff} (μm)	Total volume of particles[#] ($\times 10^7$ μm^3 cm^{-2})	Number Coincidences M_c	Sigma epsilon squared ε^2	Relative error (%) E_{rel}
0.00	1.33-0.00i	0.19	1.4	2.7	3.8	3.5×10^{-6}	4.1×10^{2}
0.25	1.53-0.19i	0.36	1.2	2.3	3.6	7.5×10^{-6}	2.1×10^{1}
0.50	1.73-0.42i	0.63	1.0	3.2	4	1.3×10^{-5}	2.5×10^{1}
0.55	1.76-0.47i	0.66	1.03	2.0	3.6	8.2×10^{-6}	2.3×10^{1}
0.60	1.80-0.52i	0.70	1.01	1.9 (304)	3.6	7.7×10^{-6}	2.3×10^{1}
0.65	1.83-0.57i	0.75	0.98	3.9 (644)	3.8	7.8×10^{-6}	2.3×10^{1}
0.75	1.89-0.69i	0.84	0.88	1.6 (280)	3.8	9.0×10^{-6}	1.8×10^{1}
1.00	2.00-1.00i	1.01	1.0	6.2	3.4	3.1×10^{-5}	1.4×10^{1}

[#] Values in brackets represent the corresponding approximate mass of aerosol in μg m^{-3} for our best estimate of aerosol composition, assuming an appropriate aerosol density considering a black carbon density of 2 g cm^{-3} (as for the Kuwait oil-fire aerosol, Nakajima *et al*. 1996), water density of 1 g cm^{-3} and a plume depth of 1000 m (based on aircraft observations; Targa *et al*. 2006).

Table 3. Mean values and standard deviations (68%-confidence intervals) of the column amounts at different measurement positions (these values will likely be slightly overestimated due to the effects of multiple scattering - see footnote) Corresponding background levels under clear and cloudy sky are given for comparison. The values in brackets underneath each value correspond to the mixing ratio (ppmv) within in the plume that each of these means correspond to assuming the plume is ~200 m in depth (based on near-source aircraft observations; Targa *et al.* 2006).

Gas	Column amount (molecules $cm^{-2} \times 10^{16}$)						
	Dataset[+]						
	HH1	HH2	HH3	HH4	HH5	Background clear sky[*]	Background cloudy sky[*]
NO_2	7.6 ± 5.9[#] (0.15)	6.1 ± 0.71 (0.12)	7.0 ± 1.1 (0.14)	7.5 ± 1.3 (0.15)	7.3 ± 1.0 (0.14)	2.7 ± 1.1	3.1 ± 2.5[#]
SO_2	3.4 ± 1.5 (0.07)	3.8 ± 0.75 (0.08)	3.1 ± 0.80 (0.06)	3.6 ± 1.2 (0.07)	3.1 ± 1.3 (0.06)	2.2 ± 0.9	-1.2 ± 2.5[#]
HONO	0.22 ± 0.42[#] (0.01)	1.1 ± 0.35 (0.02)	1.1 ± 0.19 (0.02)	0.88 ± 0.25 (0.02)	0.89 ± 0.24 (0.02)	0.18 ± 0.40[#]	0.27 ± 0.83[#]
HCHO	7.7 ± 3.3 (0.15)	10.6 ± 3.7 (0.20)	7.9 ± 1.6 (0.15)	8.1 ± 1.9 (0.16)	6.8 ± 2.5 (0.13)	2.8 ± 2.5[#]	3.5 ± 4.0[#]
CS_2	4.9 ± 16.0[#] (0.05)	2.1 ± 5.7[#] (0.04)	2.4 ± 6.4[#] (0.05)	2.7 ± 4.8[#] (0.05)	0.80 ± 6.5[#] (0.02)	1.8 ± 1.5[#]	2.6 ± 3.1[#]
Number of spectra	166	92	515	231	258	65	112

[+] Condition of the plume: HH1 (dark, opaque, variable density), HH2 (grey, dense, uniform), HH3 (dense, opaque, uniform), HH4 (brown, transparent, variable density), HH5 (transparent). The lack of significant systematic variation in column amount with plume condition suggests that multiple scattering only introduces minor errors in these values.

[#] These mean values may not appear statistically significant because 68%-confidence intervals include zero. However, because we are considering time variations of strongly fluctuating quantities, this is not the case and in fact much of the time the measured plume column amounts significantly exceeded corresponding background levels even when "cloudy" background was considered.

[*] The background levels measured under cloudy sky (layer of low Stratocumulus opacus) tend to be higher than corresponding values measured under clear sky. There are at least two reasons for this. Firstly, with a constant total integration time the signal to noise ratio is lower for measurements taken under cloudy sky. Secondly, multiple scattering within the cloud layer lengthens the photon paths increasing absorption (Pfeilsticker *et al.* 1997; Wagner *et al.* 2002).

Table 4. Mean values and standard deviations (68%-confidence intervals) estimations of molar ratios with NO_2 for the fitted gasses at different measurement positions. Assuming weak absorption for all measured gases we can suppose that they have almost the same air mass factors and thus the molar ratios can be assumed to be reliable despite any effects of multiple scattering.

Molar Ratio (X/NO_2)	Mean values						
	HH1	HH2	HH3	HH4	HH5	Background clear sky	Background cloudy sky
SO_2	0.474 ± 0.399	0.623 ± 0.143	0.443 ± 0.134	0.480 ± 0.180	0.425 ± 0.187	0.815 ± 0.470	0.387 ± 0.865
HONO	0.029 ± 0.060	0.180 ± 0.061	0.157 ± 0.037	0.117 ± 0.039	0.122 ± 0.037	0.067 ± 0.151	0.087 ± 0.277
HCHO	1.013 ± 0.898	1.738 ± 0.639	1.129 ± 0.289	1.080 ± 0.315	0.932 ± 0.365	1.037 ± 1.018	1.129 ± 1.579
CS_2	0.645 ± 2.164	0.344 ± 0.935	0.343 ± 0.916	0.360 ± 0.643	0.110 ± 0.891	0.667 ± 0.618	0.839 ± 1.207

Figure 1.

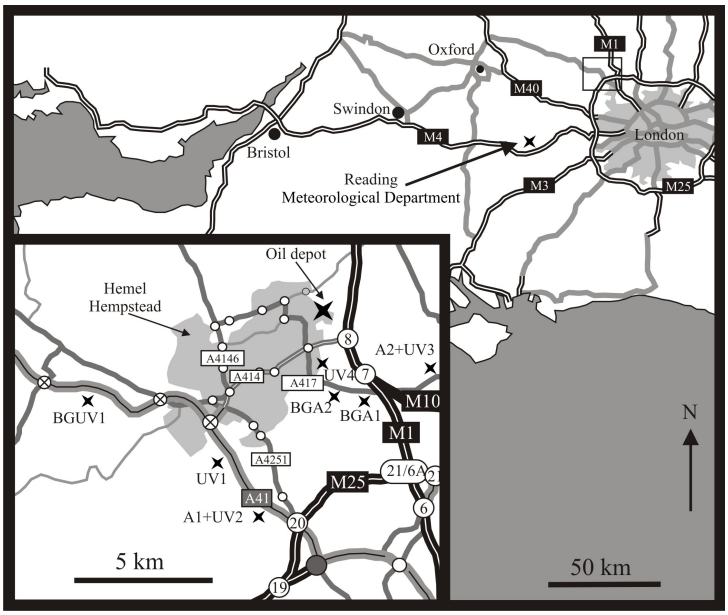
Oxford
M1
M40
Swindon
M4
London
Bristol
Reading
Meteorological Department
M3
M25
Oil depot
Hemel
Hempstead
A4146
A414
A417
8
A2+UV3
UV4
7
M10
BGUV1
BGA2
BGA1
M1
A4251
UV1
21/6A
M25
A41
A1+UV2
20
6
5 km
19
N
50 km

Figure 2.

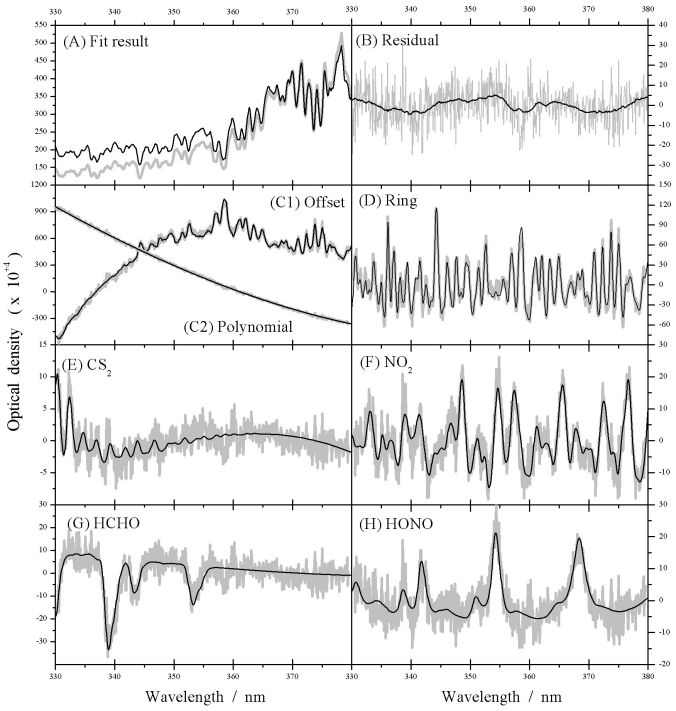
(A) Fit result
(B) Residual
(C1) Offset
(C2) Polynomial
(D) Ring
(E) CS2
(F) NO2
(G) HCHO
(H) HONO
Optical density (x 10-4)
Wavelength / nm
Wavelength / nm

Figure 3.

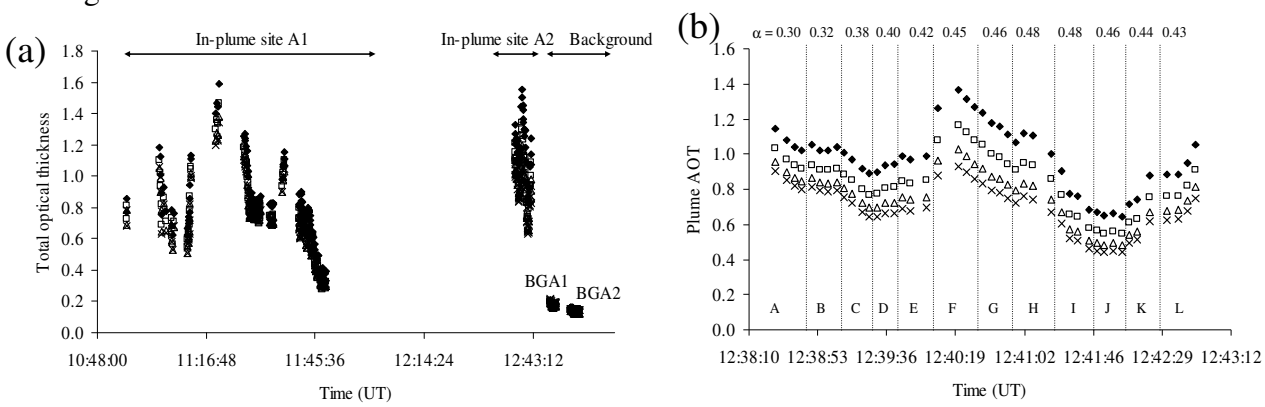
(a)
In-plume site A1
In-plume site A2
Background
BGA1
BGA2
Total optical thickness
Time (UT)
(b)
α = 0.30 0.32 0.38 0.40 0.42 0.45 0.46 0.48 0.48 0.46 0.44 0.43
Plume AOT
A B C D E F G H I J K L
12:38:10 12:38:53 12:39:36 12:40:19 12:41:02 12:41:46 12:42:29 12:43:12
Time (UT)

Figure 4.

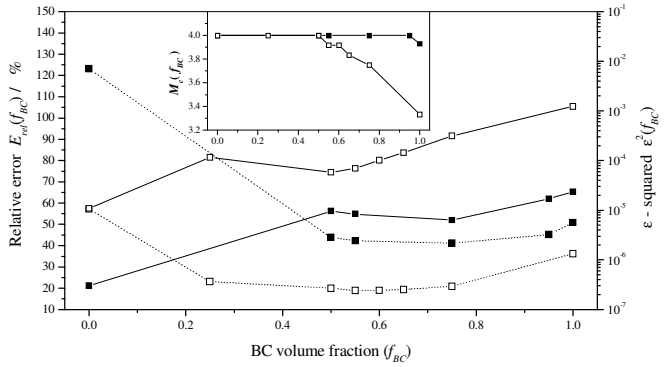
Relative error $E_{rel}(f_{BC})$ / %
ε - squared $\varepsilon^2(f_{BC})$
BC volume fraction (f_{BC})
$M_w(f_{BC})$

Figure 5.

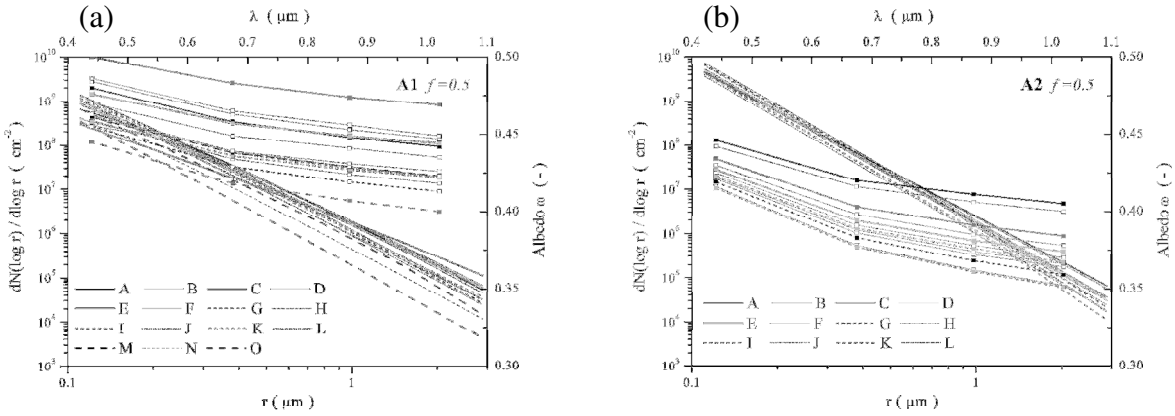
(a)
λ (μm)
A1 f=0.5
dN(log r) / dlog r (cm⁻²)
Albedo ω (-)
r (μm)
A B C D
E F G H
I J K L
M N O
(b)
λ (μm)
A2 f=0.5
dN(log r) / dlog r (cm⁻²)
Albedo ω (-)
r (μm)
A B C D
E F G H
I J K L

Figure 6.

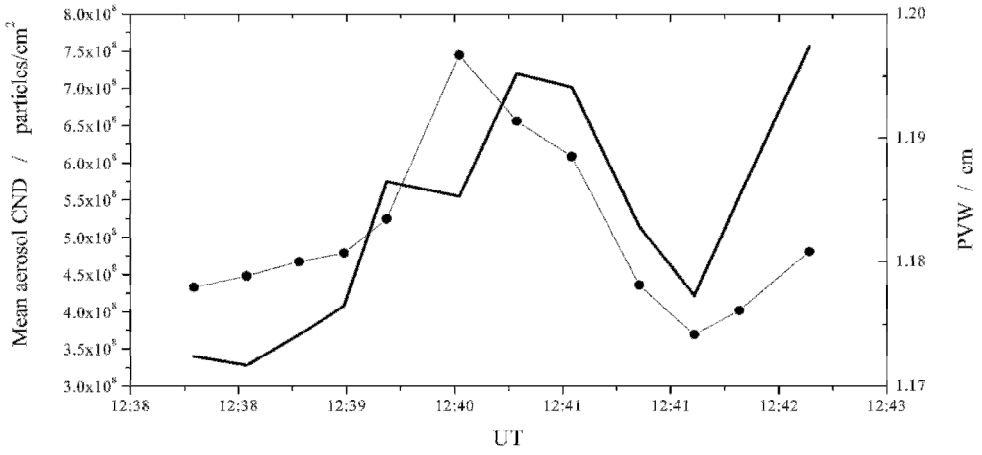
Mean aerosol CND / particles/cm^2
8.0x10^8
7.5x10^8
7.0x10^8
6.5x10^8
6.0x10^8
5.5x10^8
5.0x10^8
4.5x10^8
4.0x10^8
3.5x10^8
3.0x10^8
1.20
1.19
1.18
1.17
PWV / cm
12:38
12:38
12:39
12:40
12:41
12:41
12:42
12:43
UT

Figure 7.

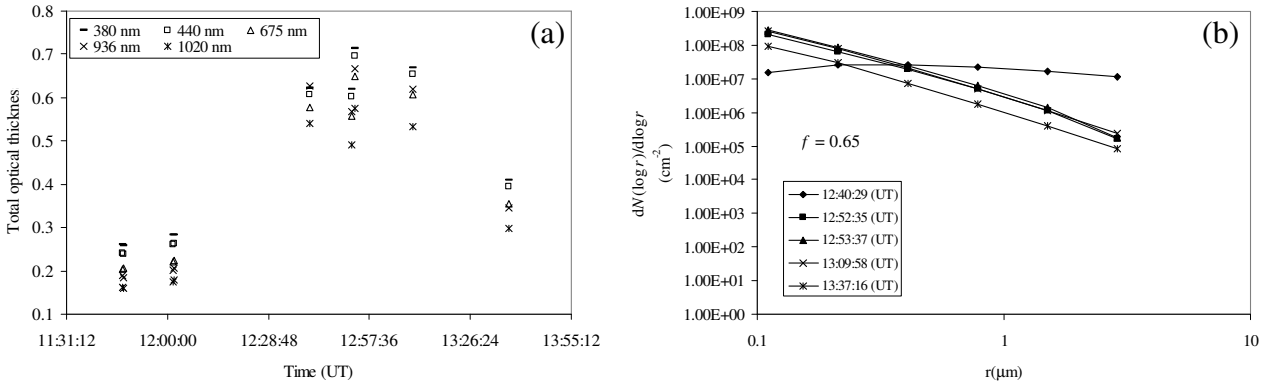
(a)
380 nm
440 nm
675 nm
936 nm
1020 nm
Total optical thicknes
Time (UT)
11:31:12
12:00:00
12:28:48
12:57:36
13:26:24
13:55:12
(b)
f = 0.65
12:40:29 (UT)
12:52:35 (UT)
12:53:37 (UT)
13:09:58 (UT)
13:37:16 (UT)
r(μm)

Figure 8.

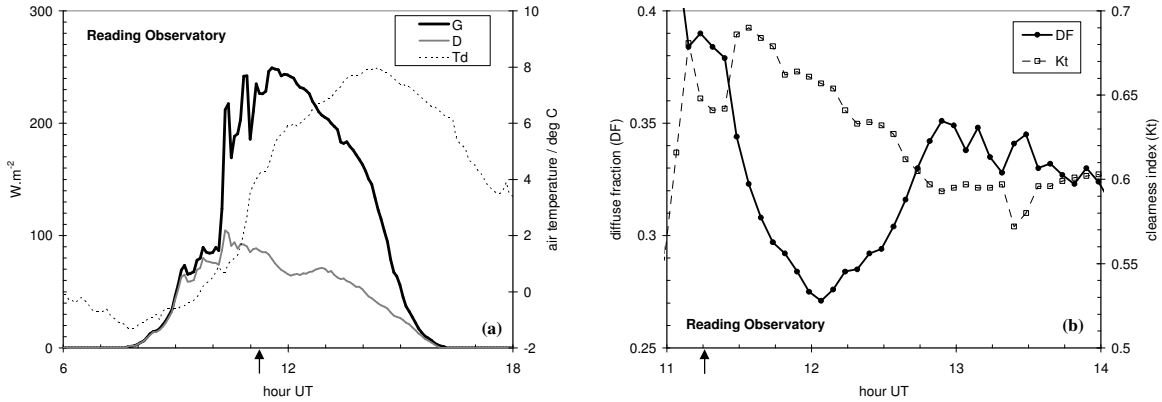
Reading Observatory
G
D
Td
W.m-2
air temperature / deg C
hour UT
(a)
diffuse fraction (DF)
cleamess index (Kt)
DF
Kt
Reading Observatory
(b)
hour UT